micro

MDPI

Article

Magnetic Aspects and Large Exchange Bias of $Ni_{0.9}Co_{0.1}$/NiCoO Multilayers

Dimitrios I. Anyfantis [1], Nikos Kanistras [1], Camillo Ballani [2], Alexandros Barnasas [1], Vassilios Kapaklis [3], Georg Schmidt [2], Evangelos Th. Papaioannou [2] and Panagiotis Poulopoulos [1,*]

[1] Department of Materials Science, School of Natural Sciences University of Patras, Rio, 26504 Patras, Greece; up1057157@upatras.gr (D.I.A.); ndkanistras@gmail.com (N.K.); mparnalex@gmail.com (A.B.)

[2] Institut für Physik, Martin-Luther University Halle-Wittenberg Von-Danckelmann-Platz 3, 06120 Halle, Germany; camillo.ballani@physik.uni-halle.de (C.B.); georg.schmidt@physik.uni-halle.de (G.S.); evangelos.papaioannou@physik.uni-halle.de (E.T.P.)

[3] Department of Physics and Astronomy, Uppsala University, Box 516, SE-751 20 Uppsala, Sweden; vassilios.kapaklis@physics.uu.se

* Correspondence: poulop@upatras.gr

Abstract: Ultrathin films of $Ni_{0.9}Co_{0.1}$ were grown by radio frequency magnetron sputtering. By means of a periodic natural oxidation procedure they were transformed into $Ni_{0.9}Co_{0.1}$/NiCoO multilayers. Room temperature hysteresis loops recorded via the magneto-optic Kerr effect have revealed over all in-plane magnetic anisotropy due to magnetostatic anisotropy. Mild thermal annealing at 250 °C enhanced a tendency for perpendicular magnetic anisotropy, mainly due to an increase of the uniaxial volume anisotropy term. Spin reorientation transition, exchange bias larger than 700 Oe, and strong coercivity enhancement were observed via a superconducting quantum interference device at low temperatures after field cooling.

Keywords: magnetic multilayers; magnetic anisotropy; exchange bias; spintronics; NiCoO

check for updates

Citation: Anyfantis, D.I.; Kanistras, N.; Ballani, C.; Barnasas, A.; Kapaklis, V.; Schmidt, G.; Papaioannou, E.T.; Poulopoulos, P. Magnetic Aspects and Large Exchange Bias of $Ni_{0.9}Co_{0.1}$/NiCoO Multilayers. *Micro* **2021**, *1*, 43–54. https://doi.org/10.3390/micro1010005

Received: 14 June 2021
Accepted: 29 June 2021
Published: 2 July 2021

1. Introduction

The field of nanomagnetics where very small-scale structures such as ultrathin (few atomic layer) films of ferromagnetic material are involved has been of great interest for the last few decades [1]. Magnetic recording media [2] and sensors and actuators based on spintronics [3–5] are the predominant applications for magnetic thin films and multilayers. Remarkable phenomena such as exchange bias at ferromagnetic/antiferromagnetic interfaces [6,7], perpendicular magnetic anisotropy (PMA) in thin films [8], and giant and tunnel magnetoresistance [9,10] are currently used in spintronic applications. Recent works reveal that oxides and, more specifically, transition metal/oxide ultrathin films and oxide interfaces are a central component in the development of modern electronic system concepts [11]. Since it has been observed in a wide variety of amorphous or crystalline oxides, including AlOx, MgO, TaOx, CoNiO, etc., PMA has been found to be quite common at magnetic metal/oxide interfaces [8,12–16].

Cobalt and nickel are two of the three elements (iron being the third) that are strongly ferromagnetic at ambient temperature. Co, Ni, and NiCo thin films are important for both, basic and applied, research [17–19]. NiO and NiCoO have both a simple slightly distorted NaCl-type structure and are classified in the categories of anti-ferromagnetic materials. At room temperature, NiCoO has been used as an AFM material to induce an effective exchange bias (EB) [20]. Exchange bias refers to the zero-field axis shift of the hysteresis loop. It was discovered in surface-oxidized Co particles by Meiklejohn in 1956 [21]. In order to research EB, often ferromagnetic/antiferromagnetic (FM/AFM) bilayers have been investigated due to their technical significance and probably due to their convenient form. When the FM/AFM bilayer is cooled through the Néel temperature of the AFM layer under an external magnetic field, the exchange interaction at the interface of ferromagnetic (FM) and antiferromagnetic (AFM) layers produces unidirectional anisotropy [7,22,23]. Recently, Spadaro et al. synthesized films of magnetic Ni/NiO core–shell nanoparticles to obtain large EB. By varying the thickness of the shell, they have the ability to adjust the EB effect [24].

By following an alternative procedure, one may fabricate metal/metal oxide multilayer films, namely Ni/NiO [25–28] and Co/CoO [29], using only one sputtering head. The method uses natural oxidization, which results in an ultrathin oxide layer of constant thickness (of about 1.4 ± 0.2 nm) throughout the whole multilayer film. We were able to fabricate heterostructure multilayers with excellent sequencing using this simple and cost-effective procedure. The magnetic and structural properties of these multilayers were previously investigated after mild thermal annealing [30,31]. Both systems showed a small degradation in multilayer quality after thermal annealing. In Ni/NiO multilayers, the PMA is enhanced to a great extent due to partial recrystallization of NiO layers after annealing [30]. The Co/CoO films exhibit a small increase in coercivity without considerable changes in their anisotropy taking place [31].

In the current work, the correlation between magnetic anisotropy and thermal annealing of $Ni_{0.9}Co_{0.1}$/NiCoO multilayers is investigated. All the samples were prepared at relatively low argon pressure (2×10^{-3} mbar) in order to minimize roughness at the NiCo and NiCoO interfaces. This is confirmed by structural characterization using X-ray reflectivity (XRR). The magnetic characterization showed that the samples exhibit in-plane anisotropy with some of them showing the phenomenon of inverted hysteresis [32] in the loops for out-of-plane magnetic field. All the multilayers demonstrate some positive interface anisotropy. Last, but not least, a spin reorientation transition (SRT), exchange bias and strong coercivity enhancement were observed with the field applied in- and out-of-plane at low temperatures after field cooling.

2. Materials and Methods

Thin NiCo alloy films were deposited by radio frequency (rf) magnetron sputtering (at 30 W) in a vacuum chamber with a base pressure of 3×10^{-7} mbar. The samples were grown on the native oxide of Si(100) wafers and corning glass under low Ar pressure of 2×10^{-3} mbar. The sputtering gas was pure Argon (99.999 at%). For the formation of the NiCo alloy, a Co foil with small randomly distributed holes was placed on a Ni foil which was placed on the magnetron's head. The alloy composition can be adjusted by changing the number of holes, for example, see [33]. The composition of the samples was determined by energy-dispersive X-ray spectroscopy (EDS). This system, which is integrated into a scanning electron microscopy (SEM), has detected only cobalt, nickel, and oxygen in the multilayer films, with no trace of nitrogen. After each NiCo layer was deposited, air was allowed to flow inside the chamber for about 1 min through a fine valve at a partial pressure of about 2.5×10^{-3} mbar. Another NiCo layer was deposited on top of it and again oxidized. This sequence was repeated until the desired number of multilayer periods was achieved. Using this technique, multilayered films [NiCo (x: 1–6.8 nm)/NiCoO (1.4 nm)] $\times$ N with N periods ranging from 6 to 21 and total film thicknesses of about 50 nm were created, as usually thicker multilayers show a larger density of defects [26]. A pre-calibrated quartz balance system (Inficon XTM/2) was used to measure the thickness of the films in situ with an accuracy of 0.1 nm. The deposition rate was kept constant at 0.08 nm/s.

X-ray reflectivity (XRR) measurements were carried out in a Bede D1 X-ray diffractometer equipped with a Cu X-ray source operated at 35 mA and 50 kV, a Göbel mirror, and a 2-bounce-crystal on the incidence side. Furthermore, a circular mask (5 mm) as well as an incidence and a detector slit (both 0.5 mm) were used. The X-rays were detected with a Bede EDRc X-ray detector. The morphology of a NiCo/NiCoO multilayer was probed by atomic force microscopy (AFM) performed with the help of a multimode microscope with a Nanoscope IIIa controller and a 120×120 μm magnet—free scanner

(Model AS-130VMF) developed by Digital Instruments. The microscope was operated in the non-contact (tapping) mode [34].

The magnetic characterization of the multilayers was carried out using a home-made magneto-optic Kerr effect (MOKE) magnetometer [35] to record hysteresis loops with the applied field parallel (longitudinal-) and perpendicular to the film plane (polar-geometry) at room temperature (R.T.). In the temperature range of 4–300 K, a selected sample was measured via a Quantum Design SQUID VSM magnetometer. The measurement protocol included initially cooling down in field, setting the temperature value, and then the magnetic hysteresis loop runs from +maximum saturation field to -maximum field and back to +maximum field. In such a way, we exclude any experimental factor that can influence the magnetization reversal.

3. Results and Discussion

3.1. Multilayer Structural Characterization

In Figure 1, X-ray reflectivity (XRR) patterns for two NiCo/NiCoO multilayers are plotted. The number N of multilayer periods are 10 and 17, respectively. Both patterns consist of Bragg peaks numbered as n = 1, 2, etc. These are the peaks with the multilayer period Λ as the scattering unit rather than the individual crystallographic planes. Their presence confirms the formation of multilayers.

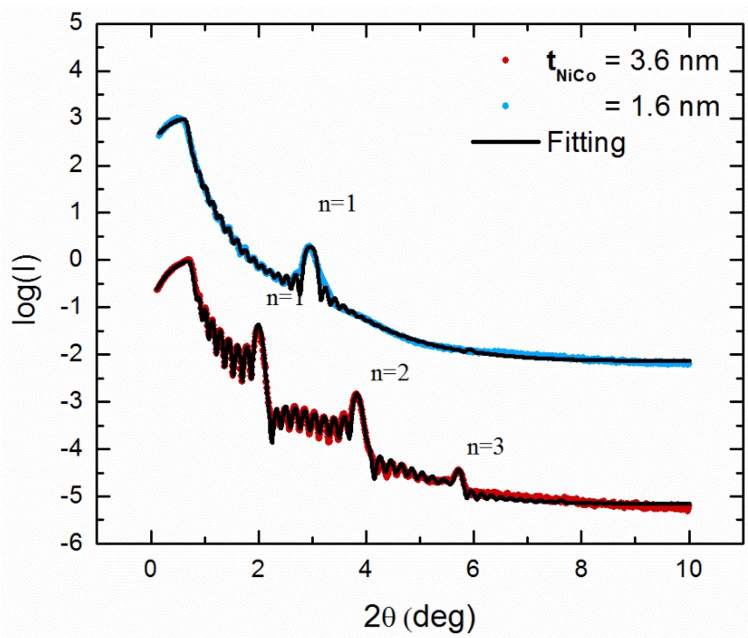

Figure 1. XRR patterns (logarithm of the X-ray Intensity I as a function of angle 2θ) for two NiCo/NiCoO multilayers with 17 (top) and 10 (bottom) repetitions (colored data points). Both samples have a total thickness of about 50 nm. The fitted patterns using the GenX code are also shown (continuous lines). From the fitting, the t_{NiCoO} was found to be 1.4 ± 0.2 nm.

Using the modified Bragg Equation (1) [36],

$$2t(\sin \theta_{n+1} - \sin \theta_n) = \lambda \tag{1}$$

where θ_{n+1} and θ_n are the positions of two successive Kiessig fringes, we can determine the total film thickness t. The thickness t of the multilayers is indeed ~50–52 nm. The fitting of the data is done using the GenX software package [37]. GenX fittings allow us to determine the scattering length density profile of the film stack, relating to individual layer thicknesses and roughnesses. In our fitting process, the NiCoO thickness was found to be 1.4 ± 0.2 nm. A detailed XRR study has revealed that the thickness of the oxide layer is almost constant and reproducible [27]. The multilayers are structurally and magnetically repeatable. This is due to the fact that both Ni and Co, unlike Fe, form protective oxide layers [26]. We have found that the multilayer consisting of N = 10 repetitions has a period of Λ = 5.0 nm, while the one with N = 17 repetitions has Λ = 3.0 nm (Figure 1). Both multilayers show an intense first Bragg peak. Many Kiessig fringes appear between the Bragg peaks and extend far out in the two-theta plots showing a very small film roughness [38]. In the simulations of the experimental data, the roughness profile is implemented as a sinusoidal modulation of the layer thickness. The root-mean-square (RMS) roughness values of NiCo and NiCoO layers are under 1 nm (0.57 and 0.75 nm, respectively for the sample with 17 repetitions, and 0.56 and 0.56 nm, respectively for the sample with 10 repetitions).

Finally, for completeness sake, in Figure 2 we present indicatively the AFM image of the surface of a multilayer with the thickest NiCo layers. One may see nanograins of about 10 nm large, quite homogeneous in terms of size. The RMS roughness is 0.45 nm.

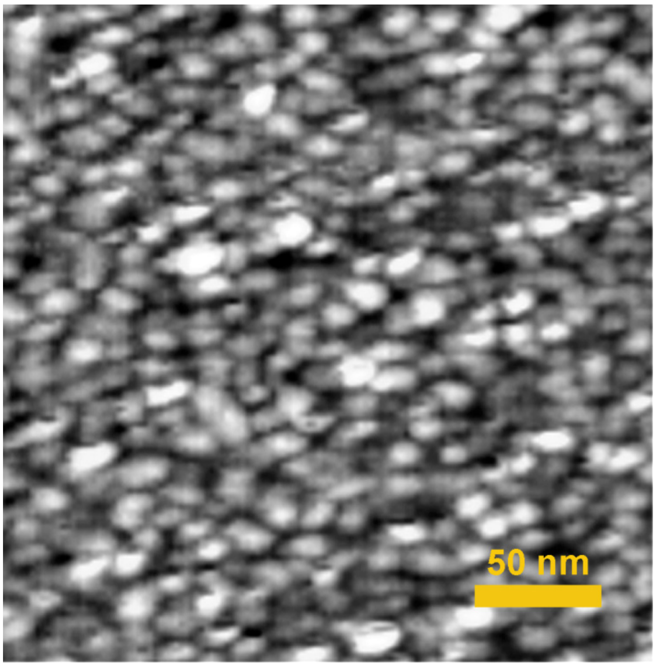

Figure 2. AFM image 250 × 250 nm^2 of the surface of a NiCo/NiCoO multilayer with t_{CoNi} (6.8 nm) thickness layer and six repetitions.

3.2. Magnetic Characterization

Figures 3a, 4a and 5a show the magnetic hysteresis loops recorded by MOKE for three NiCo/NiCoO multilayers measured in the longitudinal (polar) geometry where the external magnetic field is applied parallel (perpendicular) to the film plane at R.T. The calibration of the *Y*-axis of MOKE loops in magnetization units was performed by taking 90% of the contribution of the magnetization of Ni magnetization from a Ni/NiO multilayer with the same individual layer thickness determined by SQUID [27], and adding 10% of the magnetization of bulk Co. One NiCo/NiCoO multilayer was measured by SQUID and the experimental result for the magnetization compared within 5% to our calculation approach verifying the validity of it. The easy magnetization axis for all samples is parallel to the film plane. Polar magnetization hysteresis loops show a hard-axis behavior. The saturation field H_S is close to 5.5 kOe for multilayers with relatively thick NiCo layers, which decreases as the individual layer thickness t_{NiCo} decreases, although some slight hysteresis occurs. This observation may indicate the presence of a week PMA trend in the samples. When the external field was applied in the film plane, the majority of the loops appeared perfectly rectangular and the saturation is completed at about 0.5 kOe at maximum. After mild thermal annealing at 250 °C for 90 min on these samples, one may observe considerable changes in saturation and coercivity (see Figures 3b, 4b and 5b).

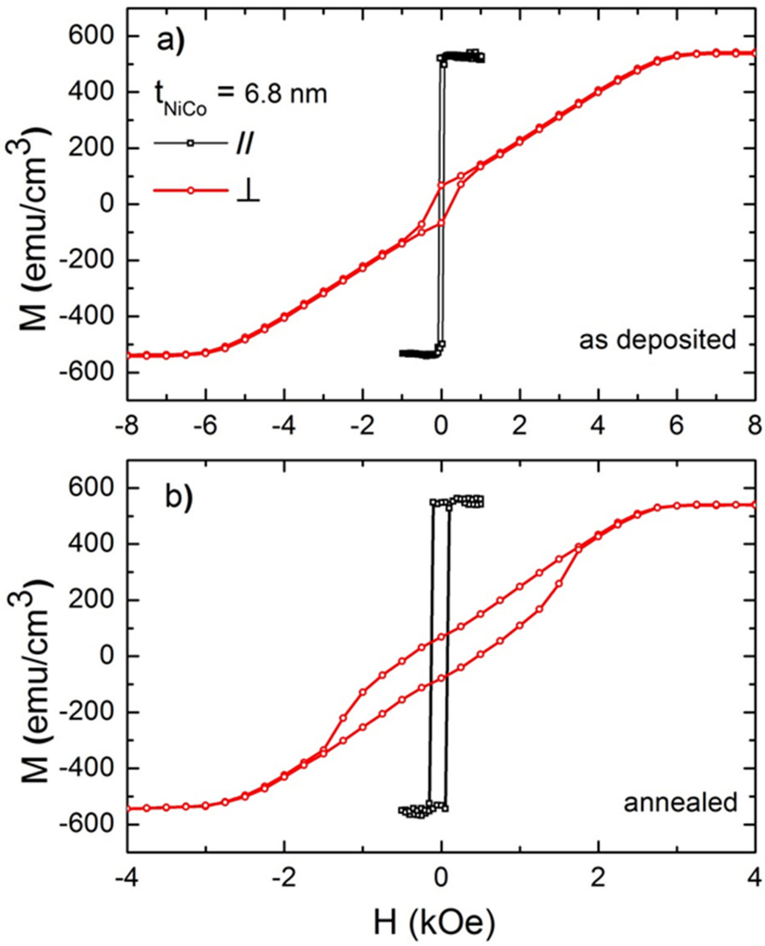

Figure 3. MOKE hysteresis loops under perpendicular (red circles) and parallel (black circles) applied magnetic fields for a NiCo/NiCoO multilayer with t_{CoNi} (6.8 nm) thickness layer and six repetitions (**a**) in the as-deposited state and (**b**) after thermal treatment at 250 °C for 90 min.

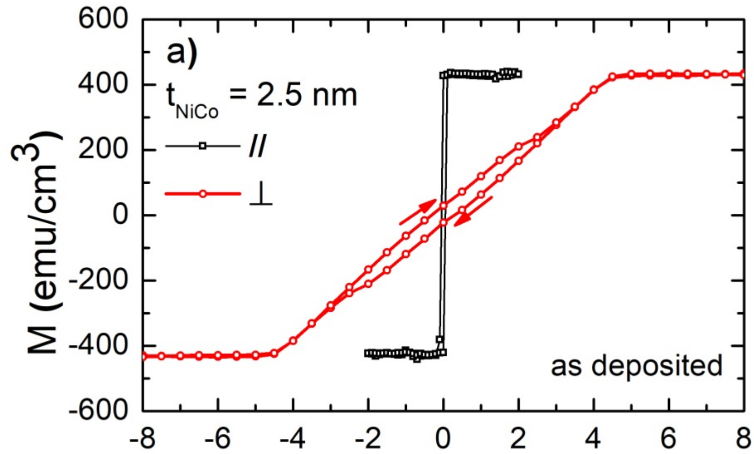

Figure 4. *Cont.*

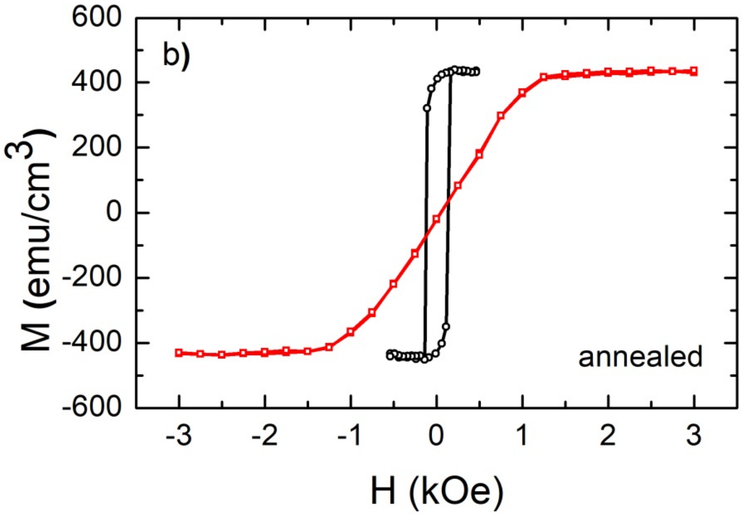

Figure 4. MOKE hysteresis loops for perpendicular (red circles) and parallel (black circles) applied magnetic fields for a NiCo/NiCoO multilayer with t_{CoNi} (2.5 nm) thickness layer and 13 repetitions (**a**) in the as-deposited state and (**b**) after thermal treatment at 250 °C for 90 min. This sample showed an inverted hysteresis loop with negative remanence in the polar geometry in the as-deposited state.

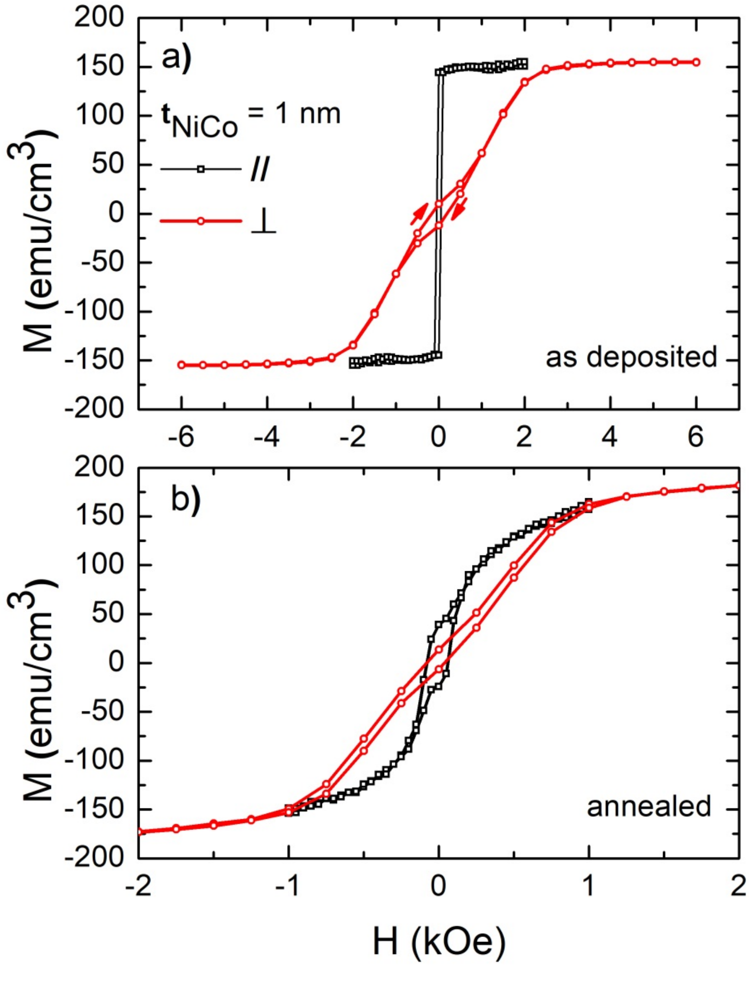

Figure 5. MOKE hysteresis loops for perpendicular (red circles) and parallel (black circles) applied magnetic fields for a NiCo/NiCoO multilayer with t_{CoNi} (1 nm) thickness layer and 21 repetitions (**a**) in the as-deposited state and (**b**) after thermal treatment at 250 °C for 90 min. This sample showed an inverted hysteresis loop with negative remanence in the polar geometry in the as-deposited state.

The product $K_{eff} \times t_{NiCo}$ as a function of t_{NiCo} is plotted in Figure 6, where K_{eff} denotes the so-called effective anisotropy normalized per NiCo-volume. It includes both long-range dipolar interactions (magnetostatic anisotropy) and spin-orbit interactions that result in anisotropic magnetic behavior (magnetic anisotropy energy) [39]. The magnetic anisotropy energy of ultrathin films and multilayers is commonly divided into two terms: Volume K_V and surface K_S. Magnetostatic anisotropy is also a volume term. As a first approximation, the magnetostatic anisotropy (though of different physical origins) will be included in the K_V definition. The following equation can then be written as follows (2):

$$K_{eff} \times t_{NiCo} = K_V \times t_{NiCo} + 2K_S \tag{2}$$

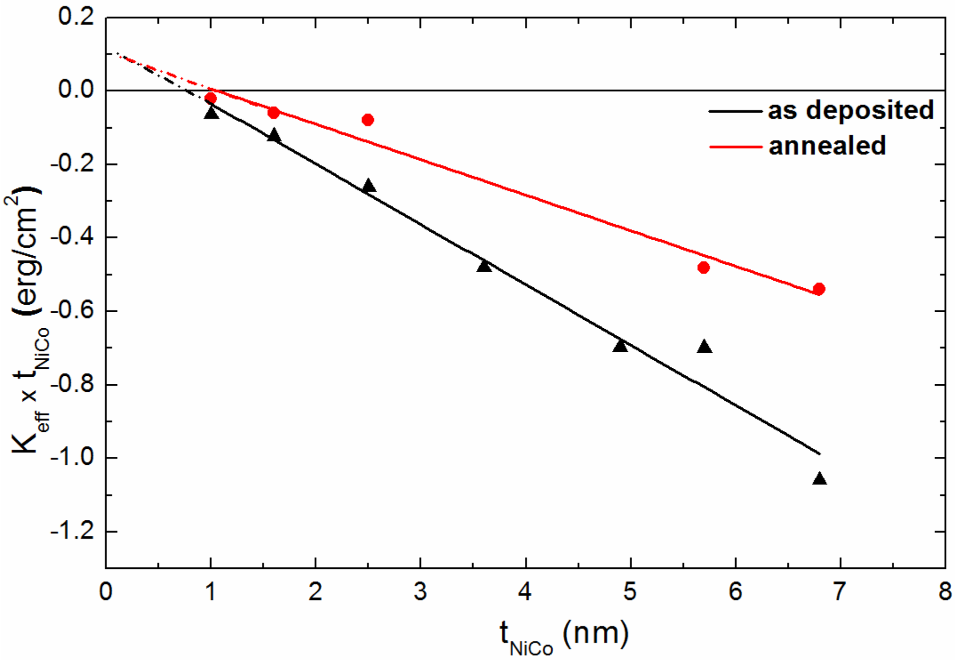

Figure 6. Plot of the effective magnetic anisotropy constant $K_{eff} \times t_{NiCo}$ as a function of t_{NiCo}, for NiCo/NiCoO multilayers in the as-deposited state (black triangles) and for the annealed samples (red circles). Measurements were carried out at R.T. One may observe a considerable change in the slope of the plot for the annealed films.

For samples with $t_{NiCo} \geq 1$ nm, a linear behavior is observed (closed symbols). All data for as-deposited (triangles) and annealed (circles) films are the outcome of the analysis of MOKE measurements. From the intercept of the $K_{eff} \times t_{CoNi}$ over t_{CoNi} plot we find $K_S = 0.065 \pm 0.025$ erg/cm^2. After thermal annealing the surface anisotropy becomes $K_S = 0.052 \pm 0.018$ erg/cm^2. We observe a slight decrease, which could be due to a small additional roughness in our samples, similar to [29]. From the slope of the plot we may determine $K_V = (-1.64 \pm 0.12) \times 10^6$ erg/cm^3 (the minus sign favors in-plane magnetization).

After thermal annealing the volume anisotropy becomes $K_V = (-0.966 \pm 0.085) \times 10^6$ erg/cm^3. The decrease of the absolute value of K_V indicates a strong tendency for PMA after annealing. A quite similar effect has been observed for Ni/NiO multilayers and was attributed to partial recrystallization of the initially amorphous NiO layers [30].

In Figure 7, we show the magnetization loops for the film with $t_{NiCo} = 2.5$ nm of Figure 4a. These loops were recorded by SQUID with the external field applied perpendicular and parallel to the field plane as indicated. Figure 7a shows that at T = 140 K the overall anisotropy remains an easy-plane. (Either one applies the field in-plane along the *X*-axis or the *Y*-axis, those are arbitrarily defined, the magnetization loops are practically indistinguishable, Figure 7a. This is a typical easy-plane behavior of polycrystalline magnetic thin films, see [39] and the references therein). However, when the field is applied perpendicular to the film plane, at H_N (nucleation field) perpendicular magnetic domains should appear, as one may conclude from the shape of the loop, e.g., see [28]. At T = 4 K the perpendicular direction becomes an easy axis, as it is clearly shown in Figure 7b. Therefore, between the room temperature and 4 K a SRT occurs. We have to notice that the 4 K loops were recorded after field cooling and this is why they appear exchange-shifted.

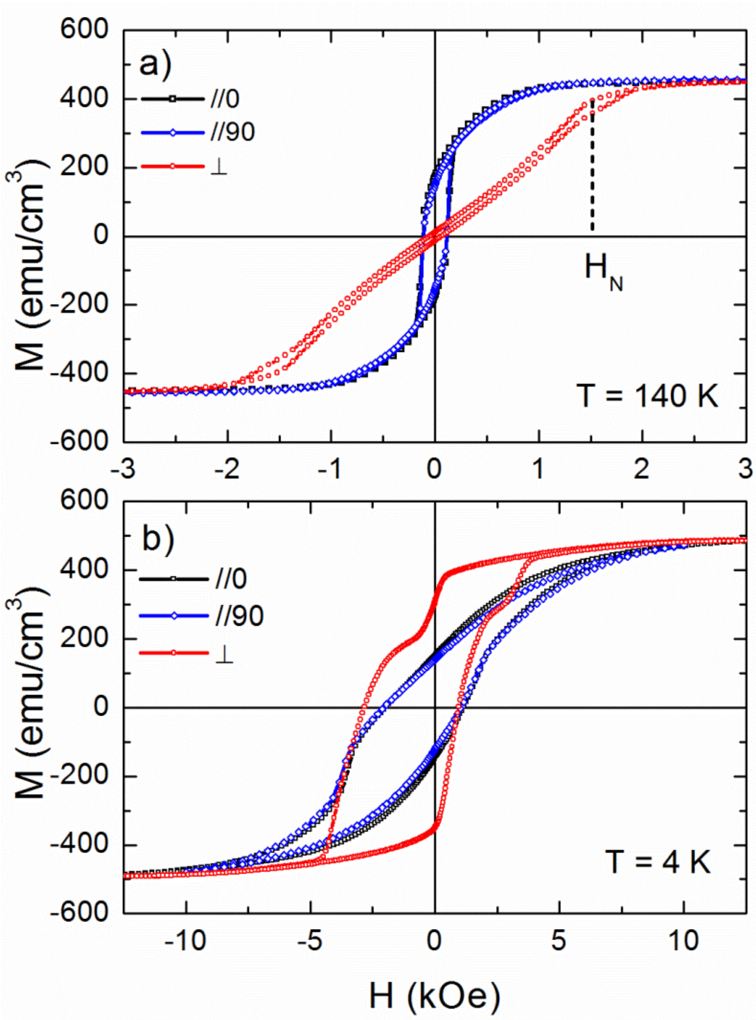

Figure 7. SQUID hysteresis loops recorded under perpendicular (red circles, H along *z*-axis) and parallel (black squares, H along *x*-axis, blue circles, H along *y*-axis) applied magnetic fields for a NiCo/NiCoO multilayer with t_{CoNi} = 2.5 nm in the as-deposited state at (**a**) 140 and (**b**) 4 K after a field cooling from 400 to 4 K.

Films with transition metal/metal oxide interfaces, such as ours, have been extensively analyzed in terms of the exchange bias phenomenon [23,24,40–44]. Furthermore, Ni-based thin films usually show smaller loop-shifts than Co-based ones [7,23]. In the present case, however, the EB field at 4 K was particularly large (H_E = 744 Oe for the perpendicular field).

Table 1 provides our values of H_E and coercivity enhancement together with the literature ones for Ni-based thin films at 4–10 K. In a recent work, A. C. Pebley et al. presented nanogranular $NiFe_2O_4$/NiO with a large shift of hysteresis loop at 5 K of about 2 kOe due to structural disorders in the ferrimagnet/antiferromagnet interfaces [45]. Systems with ferromagnet/antiferromagnet interfaces [41–44,46,47] (see Table 1) show relatively small H_E down to 100 Oe compared to our NiCo/NiCoO multilayer. This may be due to the addition of Cobalt (10 at% Co) in our samples. One has to notice that while the composition of Co is only about 10 at%, the contribution to the magnetization of the films is about three times more important as Co has a much larger magnetization than Ni.

We note that while the mechanism of exchange bias is not always the same, Table 1 serves as a collection of data for the reader.

Table 1. Summary of H_E (exchange bias field) and H_C (coercivity) enhancement for various Ni-based thin films and multilayered systems. Note that H_E was recorded at temperatures T = 4–10 K.

Material	H_E (Oe)	H_C Enhancement	Reference
$NiFe_2O_4$/NiO	2000	-	[45]
$Ni_{38.8}Co_{2.9}Mn_{37.9}Ti_{20.4}$	1200	No	[48]
NiCo/NiCoO	744	Yes	This work
$Ni_{50}Mn_{36.3}Sb_{10.4}Al_{3.3}$	611	Yes	[49]
Ni/NiO	570	No	[24]
NiO/Ni	258	Yes	[46]
$Ni_{81}Fe_{19}$/NiO	110	Yes	[41]
NiCoO/NiFe	85	-	[42]
$Ni_{49.8}Mn_{36.1}Sn_{13.9}$	41	No	[50]
Ni/NiO	40	Yes	[43]
NiFe/NiFeO	38	-	[44]
FeNi/FeMn	26	-	[47]

In Figure 8, we plot with solid lines three M(T) curves with the field applied along the film plane, for three different field values: 0, 0.1, and 1 kOe. One may see that down to 200 K the magnetic remanence is equal to the saturation magnetization, showing a rectangular-loop shape. Below about 200 K, magnetic remanence progressively decreases corresponding to the curved loops recorded with the in-plane field as a SRT is approached (see Figure 7b). For completeness, we also plot with dashed lines the corresponding three M(T) curves with the field applied along the film normal. In this case, without the field the M(T) curve is practically zero, as the film normal is a hard axis at high temperatures and at lower temperatures breaks up in to up and down magnetic domains (for example, see the shape of polar MOKE loop at 140 K, Figure 7a). Only under large fields the out-of-plane loops get progressively some considerable value of magnetization. A crossing of the in and out of-plane curves under 1 kOe occurs only at about 85 K showing that the predominant behavior is determined by PMA.

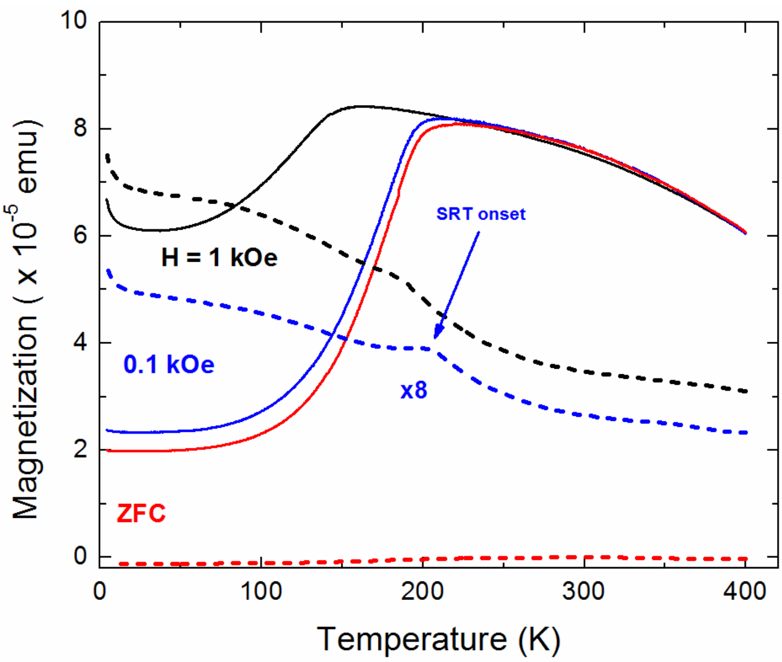

Figure 8. M(T) curves for the multilayer with t_{CoNi} = 2.5 nm in the as-deposited state after cooling from 400 to 4 K with or without in-plane (solid) or out-of-plane (dashed line) applied fields, respectively, as indicated. By an arrow we mark the onset of the SRT.

In Figure 9, we show the temperature dependence of both, EB and coercivity H_C, with the field applied parallel to the film plane. Exchange bias is relatively large (>0.3 kOe at 4 K) and becomes even larger (~744 Oe) for the out-of-plane (easy-axis) direction as Figure 7b reveals. Interestingly, H_E is slightly larger at 20 than 4 K. Such an effect has also been observed in [48] and the references therein. The exchange field of our multilayer gets very small for temperatures larger than about 60 K. This may show that the Néel temperature of antiferromagnetic NiO is placed below about 100 K due to the very small thickness of NiO layers, t_{NiO} = 1.4 nm, according to the finite-size effect, for example, see [39,51,52]. Last but not least, the coercivity at low temperatures has a significant value close to 1.4 kOe, while in the out-of-plane direction it exceeds 1.5 kOe (Figure 7b).

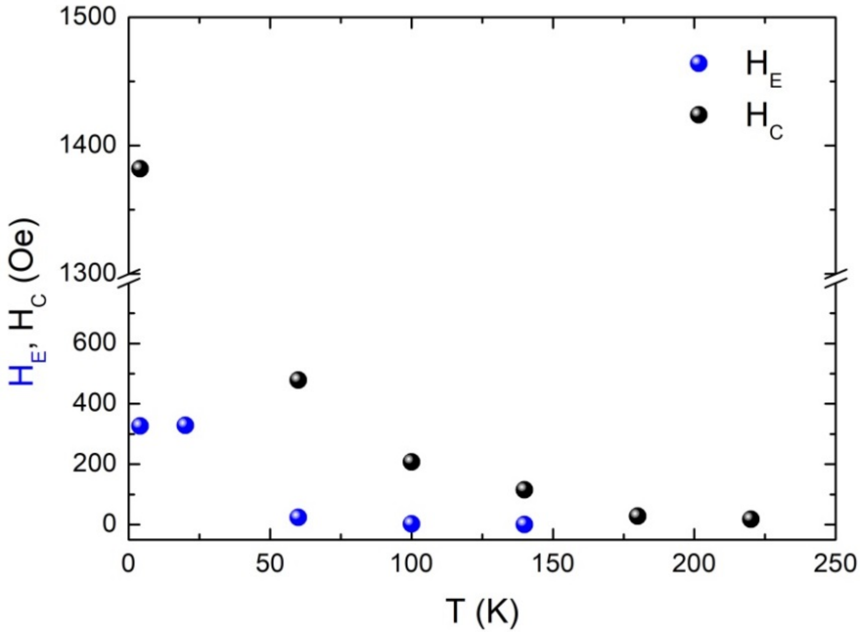

Figure 9. Temperature T dependence of exchange bias field H_E and coercivity H_C for the multilayer with t_{CoNi} = 2.5 nm in the as-deposited state and with the external field applied in the film plane.

4. Conclusions

In this work, we study the effects of Co doping on the magnetic properties of Ni/NiO multilayers. In the as-deposited state, the samples show an easy-plane behavior, typically expected for polycrystalline magnetic thin films. Annealing at temperatures up to 250 °C results in a relatively strong tendency for perpendicular magnetic anisotropy. For a multilayer with t_{CoNi} = 2.5 nm in the as-deposited state we have recorded temperature-dependent hysteresis loops. We observed a spin reorientation transition at low temperatures. After field cooling at 4 K the sample shows a substantial exchange field, which in the out-of-plane direction exceeds 700 Oe. The coexistence of PMA and EB renders this system interesting for perpendicular exchange bias applications and promotes further investigations.

Author Contributions: Conceptualization, P.P.; methodology, P.P., D.I.A., and E.T.P.; software, N.K. and V.K.; validation, P.P., E.T.P., V.K., and G.S.; formal analysis, D.I.A., N.K., A.B., and C.B.; investigation, D.I.A., N.K., A.B., and C.B.; resources, P.P., E.T.P., V.K., and G.S.; data curation, D.I.A., N.K., and C.B.; writing—original draft preparation, D.I.A.; writing—review and editing, P.P., E.T.P., V.K., and G.S.; visualization, P.P., E.T.P., V.K., and G.S.; supervision, P.P. and E.T.P.; project administration, P.P.; funding acquisition, D.I.A., P.P., and E.T.P. All authors have read and agreed to the published version of the manuscript.

Funding: The research work was supported by the Hellenic Foundation for Research and Innovation (HFRI) under the HFRI PhD Fellowship Grant (Fellowship No. 1006). The work was supported by the bilateral German-Greek Collaboration scheme for the promotion of the exchange and scientific corporation, PPP-DAAD IKYDA 2020, Project number 57547336, Title: Antiferromagnetic spintronics using novel ferromagnetic/antiferromagnetic-oxide multilayer structures.

Institutional Review Board Statement: Not applicable.

Informed Consent Statement: Not applicable.

Data Availability Statement: Data is contained within the article.

Acknowledgments: We thank V. Karoutsos for the AFM images.

Conflicts of Interest: The authors declare no conflict of interest.

References

1. Heinrich, B.; Bland, J.A.C. *Ultrathin Magnetic Structures I*, 1st ed.; Springer: Berlin/Heidelberg, Germany, 1994; pp. 1–6.
2. O'Handley, R.C. *Modern Magnetic Materials: Principles and Applications*, 1st ed.; Wiley: New York, NY, USA, 2000; pp. 676–720.
3. Freitas, P.P.; Ferreira, R.; Cardoso, S. Spintronic Sensors. *Proc. IEEE* **2016**, *104*, 1894–1918. [CrossRef]
4. Bhatti, S.; Sbiaa, R.; Hirohata, A.; Ohno, H.; Fukami, S.; Piramanayagam, S.N. Spintronics based random access memory: A review. *Mater. Today* **2017**, *20*, 530–548. [CrossRef]
5. Felser, C.; Fecher, G.H.; Balke, B. Spintronics: A challenge for materials science and solid-state chemistry. *Angew. Chem.* **2007**, *46*, 668–699. [CrossRef]
6. Schuller, I.K.; Kim, S.; Leighton, C. Magnetic superlattices and multilayers. *J. Magn. Magn. Mater.* **1999**, *200*, 571–582. [CrossRef]
7. Nogués, J.; Sort, J.; Langlais, V.; Skumryev, V.; Suriñach, S.; Muñoz, J.S.; Baró, M.D. Exchange bias in nanostructures. *Phys. Rep.* **2005**, *422*, 65–117. [CrossRef]
8. den Broeder, F.J.A.; Hoving, W.; Bloemen, P.J.H. Magnetic anisotropy of multilayers. *J. Magn. Magn. Mater.* **1991**, *93*, 562–570. [CrossRef]
9. Dieny, B.; Speriosu, V.S.; Parkin, S.S.P.; Gurney, B.A.; Wilhoit, D.R.; Mauri, D. Giant magnetoresistance in soft ferromagnetic multilayers. *Phys. Rev. B* **1991**, *43*, 1297. [CrossRef] [PubMed]
10. Moodera, J.S.; Kinder, L.R.; Wong, T.M.; Meservey, R. Large Magnetoresistance at Room Temperature in Ferromagnetic Thin Film Tunnel Junctions. *Phys. Rev. Lett.* **1995**, *74*, 3273–3276. [CrossRef] [PubMed]
11. Bibes, M.; Villegas, J.E.; Barthélémy, A. Ultrathin oxide films and interfaces for electronics and spintronics. *Adv. Phys.* **2011**, *60*, 5–84. [CrossRef]
12. Monso, S.; Rodmacq, B.; Auffret, S.; Casali, G.; Fettar, F.; Gilles, B.; Dieny, B.; Boyer, P. Crossover from in-plane to perpendicular anisotropy in Pt/CoFe/AlOx sandwiches as a function of Al oxidation: A very accurate control of the oxidation of tunnel barriers. *Appl. Phys. Lett.* **2002**, *80*, 4157–4159. [CrossRef]
13. Nistor, L.E.; Rodmacq, B.; Auffret, S.; Dieny, B. Pt/Co/oxide and oxide/Co/Pt electrodes for perpendicular magnetic tunnel junctions. *Appl. Phys. Lett.* **2009**, *94*, 012512. [CrossRef]
14. Manchon, A.; Ducruet, C.; Lombard, L.; Auffret, S.; Rodmacq, B.; Dieny, B.; Pizzini, S.; Vogel, J.; Uhlíř, V.; Hochstrasser, M.; et al. Analysis of oxygen induced anisotropy crossover in Pt/Co/M Ox trilayers. *J. App. Phys.* **2008**, *104*, 043914. [CrossRef]
15. Gao, H.; Harumoto, T.; Luo, W.; Lan, R.; Feng, H.; Du, Y.; Nakamura, Y.; Shi, J. Room temperature perpendicular exchange bias in CoNi/(Co,Ni)O multilayers with perpendicular magnetic anisotropy directly induced by FM/AFM interface. *J. Magn. Magn. Mater.* **2019**, *473*, 490–494. [CrossRef]
16. Dieny, B.; Chshiev, M. Perpendicular magnetic anisotropy at transition metal/oxide interfaces and applications. *Rev. Mod. Phys.* **2017**, *89*, 025008. [CrossRef]
17. Fukami, S.; Sato, H.; Yamanouchi, M.; Ikeda, S.; Ohno, H. CoNi Films with Perpendicular Magnetic Anisotropy Prepared by Alternate Monoatomic Layer Deposition. *Appl. Phys. Express* **2013**, *6*, 073010. [CrossRef]
18. Pan, Y.; Zhou, Y.; Zhou, Y.; Huang, Y.; Liao, Y.; Sun, S. Fabrication, lattice strain, corrosion resistance and mechanical strength of nanocrystalline nickel films. *Trans. Nonferrous Met. Soc. China* **2007**, *17*, 1225–1229. [CrossRef]
19. Gomez, E.; Pane, S.; Valles, E. Electrodeposition of Co–Ni and Co–Ni–Cu systems in sulphate–citrate medium. *Electrochim. Acta* **2005**, *51*, 146–153. [CrossRef]
20. Lin, K.-W.; Guo, J.-Y.; Liu, H.-Y.; Ouyang, H.; Chan, Y.-L.; Wei, D.-H.; Van Lierop, J. Anomalous exchange bias behavior in ion-beam bombarded NiCo/ (Ni,Co)O bilayers. *J. Appl. Phys.* **2008**, *103*, 07C105. [CrossRef]
21. Meiklejohn, W.H.; Bean, C.P. New Magnetic Anisotropy. *Phys. Rev.* **1956**, *102*, 1413. [CrossRef]
22. Altuncevahir, B.; Koymen, A.R. Positive and negative exchange bias in CoNi/Gd/CoNi trilayers and CoNi/Gd bilayers. *J. Magn. Magn. Mater.* **2003**, *261*, 424–432. [CrossRef]
23. Nogues, J.; Schuller, I.K. Exchange bias. *J. Magn. Magn. Mater.* **1999**, *192*, 203–232. [CrossRef]
24. Spadaro, M.C.; D'Addato, S.; Luches, P.; Valeri, S.; Grillo, V.; Rotunno, E.; Roldan, M.A.; Pennycook, S.J.; Ferretti, A.M.; Capetti, E.; et al. Tunability of exchange bias in Ni≅NiO coreshell nanoparticles obtained by sequential layer deposition. *Nanotechnology* **2015**, *26*, 405704. [CrossRef]

25. Poulopoulos, P.; Kapaklis, V.; Jönsson, P.E.; Papaioannou, E.Th.; Delimitis, A.; Pappas, S.D.; Trachylis, D.; Politis, C. Positive surface and perpendicular magnetic anisotropy in natural nanomorphous Ni/NiO multilayers. *Appl. Phys. Lett.* **2010**, *96*, 202503. [CrossRef]
26. Poulopoulos, P.; Pappas, S.D.; Kapaklis, V.; Jönsson, P.E.; Papaioannou, E.T.; Delimitis, A.; Trachylis, D.; Velgakis, M.J.; Meletis, E.I.; Politis, C. Growth and Magnetism of Natural Multilayers. *J. Nano Res.* **2011**, *15*, 95–103. [CrossRef]
27. Pappas, S.D.; Kapaklis, V.; Delimitis, A.; Jönsson, P.E.; Papaioannou, E.Th.; Poulopoulos, P.; Fumagalli, P.; Trachylis, D.; Velgakis, M.J.; Politis, C. Layering and temperature-dependent magnetization and anisotropy of naturally produced Ni/NiO multilayers. *J. Appl. Phys.* **2012**, *112*, 053918. [CrossRef]
28. Pappas, S.D.; Delimitis, A.; Kapaklis, V.; Papaioannou, E.T.; Poulopoulos, P.; Trachylis, D.; Velgakis, M.J.; Politis, C. Natural Nanomorphous Ni/NiO Magnetic Multilayers: Structure and Magnetism of the High-Ar Pressure Series. *J. Nano Nanotech.* **2014**, *14*, 6103–6107. [CrossRef]
29. Santarossa, F.; Pappas, S.D.; Delimitis, A.; Sousanis, A.; Poulopoulos, P. Naturally Produced Co/CoO Nanocrystalline Magnetic Multilayers: Structure and Inverted Hysteresis. *J. Nanosci. Nanotechnol.* **2016**, *16*, 4960–4967. [CrossRef] [PubMed]
30. Anyfantis, D.I.; Sarigiannidou, E.; Rapenne, L.; Stamatelatos, A.; Ntemogiannis, D.; Kapaklis, V.; Poulopoulos, P. Unexpected Development of Perpendicular Magnetic Anisotropy in Ni/NiO Multilayers after Mild Thermal Annealing. *IEEE Magn. Lett.* **2019**, *10*, 1–5. [CrossRef]
31. Anyfantis, D.I.; Kanistras, N.; Barnasas, A.; Poulopoulos, P.; Papaioannou, E.Th.; Conca, A.; Trachylis, D.; Politis, C. Effects of Thermal Annealing and Ni Addition on the Magnetic Properties of Co–CoO Multilayers. *SPIN* **2020**, *40*, 2050030. [CrossRef]
32. Flevaris, N.K.; Krishnan, R. Modulation-induced effects in magnetic multilayers: Perpendicular anisotropy, reversed hysteresis and magnetization enhancement. *J. Magn. Magn. Mater.* **1992**, *104–107*, 1760–1762. [CrossRef]
33. Sousanis, A.; Grammatikopoulos, S.; Delimitis, A.; Dracopoulos, V.; Poulopoulos, P. Localized surface plasmon resonances after selective oxidization of AuCu solid solution nanocrystalline films. *Appl. Phys. Lett.* **2015**, *107*, 011903. [CrossRef]
34. Karoutsos, V. Scanning Probe Microscopy: Instrumentation and Applications on Thin Films and Magnetic Multilayers. *J. Nanosci. Nanotechnol.* **2009**, *9*, 6783–6798. [CrossRef]
35. Kapaklis, V.; Pappas, S.D.; Poulopoulos, P.; Trachylis, D.; Schweiss, P.; Polotis, C. Structure and magnetic properties of hcp and fcc nanocrystalline thin Ni films and nanoparticles produced by radio frequency magnetron sputtering. *J. Nanosci. Nanotechnol.* **2010**, *10*, 6024–6028. [CrossRef] [PubMed]
36. Pearson, W.B.; Thompson, L.T. The Lattice Spacings of Nickel Solid Solutions. *Can. J. Phys.* **1957**, *35*, 349. [CrossRef]
37. Björck, M.; Andersson, G. GenX: An extensible X-ray reflectivity refinement program utilizing differential evolution. *J. Appl. Crystall.* **2007**, *40*, 1174–1178. [CrossRef]
38. Kiessig, H. Untersuchungen zur Totalreflexion von Röntgenstrahlen. *Ann. Phys.* **1931**, *402*, 715–768. [CrossRef]
39. Poulopoulos, P.; Baberschke, K. Magnetism in thin films. *J. Phys. Cond. Matt.* **1999**, *11*, 9495–9515. [CrossRef]
40. Blachowicz, T.; Ehrmann, A. Exchange Bias in Thin Films—An Update. *Coatings* **2021**, *11*, 122. [CrossRef]
41. McCord, J.; Mangin, S. Separation of low- and high-temperature contributions to the exchange bias in $Ni_{81}Fe_{19}$-NiO thin films. *Phys. Rev. B* **2013**, *88*, 014416. [CrossRef]
42. Martien, D.; Takano, K.; Berkowitz, A.E.; Smith, D.J. Increasing the exchange-bias field of Ni 0.5 Co 0.5 O films by microstructural control. *Appl. Phys. Lett.* **1999**, *74*, 1314. [CrossRef]
43. Domann, J.P.; Sun, W.Y.; Schelhas, L.T.; Carman, G.P. Strain-mediated multiferroic control of spontaneous exchange bias in Ni-NiO heterostructures. *J. Appl. Phys.* **2016**, *120*, 143904. [CrossRef]
44. Geshev, J.; Pereira, L.G.; Skumryev, V. Comment on "Exchange Bias Dependence on Interface Spin Alignment in a Ni80Fe20/(Ni Fe)O Thin Film". *Phys. Rev. Lett.* **2008**, *100*, 039701. [CrossRef]
45. Pebley, A.C.; Fuks, P.E.; Pollock, T.M.; Gordon, M.J. Exchange bias and spin glass behavior in biphasic NiFe2O4/NiO thin films. *J. Magn. Magn. Mater.* **2016**, *419*, 29–36. [CrossRef]
46. Fraune, M.; Rudiger, U.; Guntherodt, G.; Cardoso, S.; Freitas, P. Size dependence of the exchange bias field in NiO/Ni nanostructure. *Appl. Phys. Lett.* **2000**, *77*, 3815–3817. [CrossRef]
47. Schlenker, C.; Parkin, S.S.P.; Scott, J.C.; Howard, K. Magnetic Disorder in the Exchange Bias Bilayered FeNi-FeMn System. *J. Magn. Magn. Mater.* **1986**, *54–57*, 801–802. [CrossRef]
48. Liu, K.; Ma, S.C.; Zhang, Z.S.; Zhao, X.W.; Yang, B.; Wang, D.H.; Ur Rehman, S.; Zhong, Z.C. Giant exchange bias effect in all-3d-metal $Ni_{38.8}Co_{2.9}Mn_{37.9}Ti_{20.4}$ thin film. *Appl. Phys. Lett.* **2020**, *116*, 022412. [CrossRef]
49. Barman, R.; Singh, S.K.; Kaur, D. Enhanced exchange bias in magnetron-sputtered Ni–Mn–Sb–Al ferromagnetic shape memory alloy thin films. *Curr. Appl. Phys.* **2014**, *14*, 1755–1759. [CrossRef]
50. Vishnoi, R.; Kaur, D. Exchange bias behaviour in magnetron sputtered Ni49.8Mn36.1Sn13.9 ferromagnetic shape memory alloy thin film. *J. Alloys Comp.* **2011**, *509*, 2833–2837. [CrossRef]
51. Ambrose, T.; Chien, C.L. Finite-size scaling in thin antiferromagnetic CoO layers. *J. Appl. Phys.* **1996**, *79*, 5920. [CrossRef]
52. Gladii, O.; Frangou, L.; Forestier, G.; Seeger, R.L.; Auffret, S.; Rubio-Roy, M.; Weil, R.; Mougin, A.; Gomez, C.; Jahjah, W.; et al. Spin pumping as a generic probe for linear spin fluctuations: Demonstration with ferromagnetic and antiferromagnetic orders, metallic and insulating electrical states. *Appl. Phys. Expr.* **2019**, *12*, 023001. [CrossRef]